Analysis of Random Noise and Long-Term Drift for Tunable Diode Laser Absorption Spectroscopy System at Atmospheric Pressure

Guojie Tu, Fengzhong Dong, Yu Wang, Brian Culshaw, Zhirong Zhang, Tao Pang, Hua Xia, and Bian Wu

Abstract—The random noise and the slow drift, which respectively limit the signal-to-noise ratio and the long-term stability, of a wavelength modulated tunable diode laser absorption spectroscopy system, are critically analyzed and evaluated experimentally. The noise sources considered in detail include the noise contributions from the lock-in amplifier, detector-preamplifier combination noise, excess noise from the DFB laser, and detection cell instabilities, especially in multiple reflection long-path cells. We also analyze contributions to long-term drift and find that the drift may be significantly compensated by the use of an optical reference path. We find experimentally that a white cell with a path length of 17.5 m introduces excess noise resulting in its having a performance equivalent to 6-m single pass absorption path. The experimental system optimized using the results of this analysis and using the 17.5-m white cell is found to operate at a sensitivity of 1.5-ppmv carbon monoxide in a bandwidth of 4 Hz. The long-term zero offset drift levels measured over 8 h are found to be ∼120 ppmv without the reference optical path and are reduced to 20 ppmv using the balance path technique.

Index Terms—Remote sensing, gas absorption spectroscopy, noise analysis, stability analysis.

I. INTRODUCTION

WAVELENGTH modulated tunable diode Laser absorption spectroscopy (WM-TDLAS), which is referred to as wavelength modulation spectroscopy (WMS), has been widely used in many applications, such as air pollution monitoring, remote leak detection and isotope fraction determination, because of its high target gas selectivity and sensitivity [1]–[7].

G. Tu is with the Institute of Optic Communication Engineering, Nanjing University, Nanjing 210008, China (e-mail: tuguojie1986@163.com).

F. Dong, Y. Wang, Z. Zhang, T. Pang, H. Xia, and B. Wu are with the Anhui Institute of Optics and Fine Mechanics, Chinese Academy of Sciences, Hefei 230031, China (e-mail: fzdong@aiofm.ac.cn; bjyuwang@gmail.com; zhangzr@aiofm.ac.cn; bumianren1982@aiofm.ac.cn; huaxia@aiofm.ac.cn; bianwu@aiofm.ac.cn).

B. Culshaw is with the Department of Electronic and Electrical Engineering, University of Strathclyde, Glasgow G1 1XW, U.K. (e-mail: brianculshaw@yahoo.co.uk).
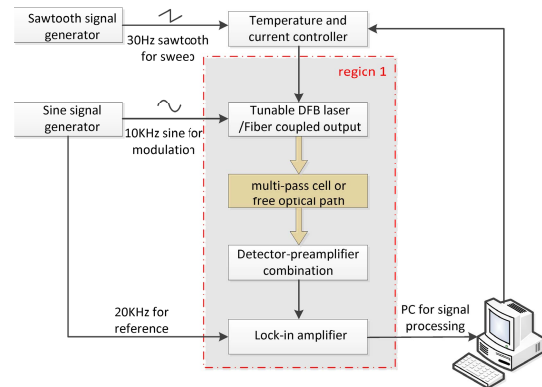
Fig. 1. Schematic diagram of a typical WMS system.

In WMS, a saw-tooth current is applied to the narrow linewidth diode laser to scan the laser wavelength, through a well characterized absorption line for the gas in question. At the same time, a high frequency sine-wave modulation current is added on the laser and a lock-in amplifier (LIA) is used to monitor the absorption signal at the second harmonic frequency (referred to as 2f-detection). By using 2f-detection to increase the detection frequency, the higher measurement signal-to-noise ratio (SNR) can be achieved due to the effective elimination of low frequency excess noises from the diode laser and detector.

In this paper, two kinds of interference factors in a WMS system are discussed. Random noise, which can be decreased by finite averaging, induces short term fluctuation in the detected gas concentration. Sources include the random noises from the electric circuit, the DFB laser and the photon detector, and the noise induced by the multi-pass cell. In contrast, long term drift which cannot be reduced by digital averaging is caused by slowly changing effects in the laser and the optical components. A detailed analysis of them is presented in next sections. We also show some methods to overcome those challenges in theory and experiments. Finally, an improved CO detection instrument is designed and its performance is compared with the original setup.

II. THE BASIC WMS SETUP

The basic setup of a WMS system is shown in Fig. 1, the marked region 1 will be described in detail as required. The system uses a fiber pigtailed DFB laser source (Agilecom, SN60001912), operating at a wavelength
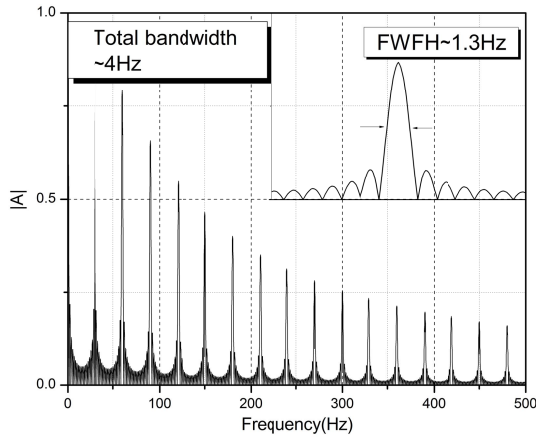
Fig. 2. The schematic diagram of the RC filter in the LIA ($\tau = 2$ ms, contributes the envelope of the filter) and 20 times data averaging (contributes the comb filter).

of 1566.639 nm, where the absorption coefficient of CO is 2.034e-23 cm^{-1}/cm^{-2} per molecule and the Full-Width at Half-Maximum (FWHM) is around 4 GHz, according to HITRAN12 [8]. The saw-tooth sweep signal is 30 Hz, 40 mA (peak-to-peak, corresponding to sweep range of 30 GHz). The sine-wave modulation current is 10 kHz, 11 mA (peak-to-peak, corresponding to frequency modulation depth of around 8.25 GHz). The optical path length of the White cell is 17.5 meters (base length is 25 centimeters). The photon detector (CETC44, GT3552T InGaAs PD, Active Area $\mathcal{C}$ 0.8 mm, Responsivity 0.9 A/W, Max Linear Power 10mW at 1550 nm) receives the transmitted light and the photocurrent is sent to the current-to-voltage convertor. In a lock-in-amplifier (LIA, analog, customized), the detector output is mixed with the reference (20 kHz) to obtain the 2f spectral signal. In this system, the 2f signal is simultaneously processed by the RC low-pass filter which is in the LIA board, and the digital averaging which produces a comb filter [9]. The longest integration time of the low-pass filter depends on the saw-tooth frequency, since the 2f spectral signal will be distorted if the integration time is too long. In contrast, the digital averaging provides a comb filter, making it very effective to depress the low-frequency noise. In our system, the integration time of RC filter is 2 ms (cut-off frequency of 80 Hz). In addition, a 20 times digital averaging is carried out, thus the final bandwidth is about 4 Hz, as shown in Fig. 2.

For the sake of random noise and slow drift analysis, the calibration CO is pumped into the multi-pass cell and recorded at first. The 2f spectral signal is normalized by light intensity [10] to reduce the intensity fluctuation effects. The random noises and long term drifts are represented in the form of ppmv.m or the equivalent absorbance.

III. NOISE ANALYSIS

The noise contribution from each system component is measured in the experiments. According to the noise distribution, the best SNR can be achieved by optimizing the system in specific applications.

The random noise contribution from LIA board is measured by using two LIA boards, shown in Fig. 3 (detailed description
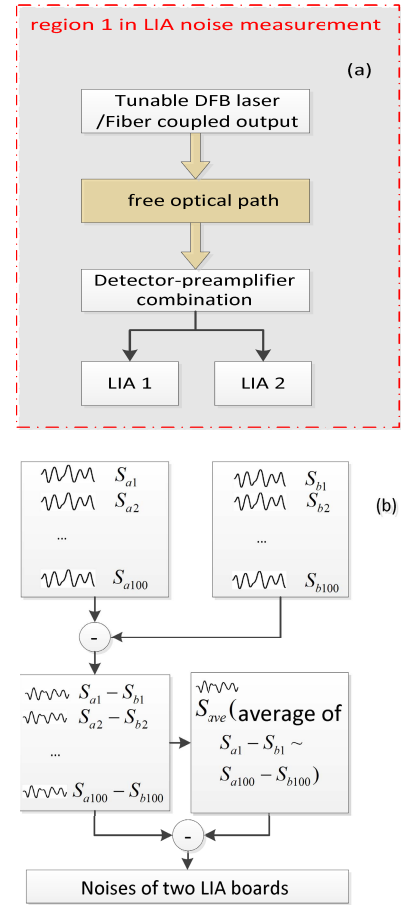

Fig. 3. (a) Shows the experimental setup of LIA noise measurement and (b) shows the schematic diagram of data processing.

of region 1 in Fig. 1). It is noted that we use the subtraction scheme instead of measuring the non-loaded LIA, since the noise contribution is dependent on the load.

In Fig. 3 (a), the light power on the photon detector is attenuated to around 1mW, which is the typical value in the system. The detector output is processed by two LIA boards which have same signal responses and noise properties. Therefore, only the noises from LIA boards can survive from the subtraction of two outputs, since these noises are uncorrelated. The power of the final noise is twice the single board's, according to property of the equipartition of energy. The schematic diagram of data processing is shown in Fig. 3 (b). One hundred groups of signals from two LIA boards are recorded, which are represented as $S_{a1} \sim S_{a100}$ and $S_{b1} \sim S_{b100}$. Therefore, $S_{a1}-S_{b1} \sim S_{a100}-S_{b100}$ are the differences of two LIAs' outputs and the average of them is represented as S_{ave}. In addition, the differences between $S_{a1}-S_{b1} \sim S_{a100}-S_{b100}$ and S_{ave} can be assumed as the summation of two LIAs' noises, which is equivalent to absorbance of $1.26 \cdot 10^{-5}$. Hence, each LIA board contributes random noise of $1.26 \cdot 10^{-5}/\sqrt{2}/\sqrt{4} = 4.46 \cdot 10^{-6}$ Hz$^{-1/2}$ (noise equivalent absorbance, NEA).

Besides of the LIA noise, the detector-preamplifier noise is measured using the arrangement shown in Fig. 4.

As described in Fig. 4 (a), a 50/50 fiber optical splitter divides the light into two equal parts, which both pass through a free optical path and be received by two detectors.
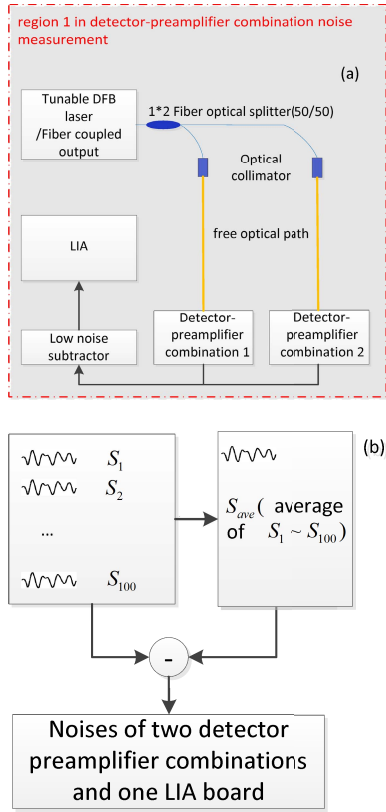
Fig. 4. (a) The balance path which is used to measure the detector-preamplifier combination noise and (b) the schematic diagram of data processing.

The spectral signals in two paths are strictly identical. This kind of scheme is called as balance detection [11]. One optical path is called as reference path, contrast to the target path. By using a low noise subtraction circuit, the difference of two outputs is obtained, which comprise the random noises from detector-preamplifier combinations and LIA board. According to [10], one detector is shadowed at first for the light intensity correction, since the power at modulation frequency is eliminated in the subtraction processing. The data demonstrates the noise equivalent absorbance of $1.33 \cdot 10^{-5}$ with bandwidth of 4 Hz, corresponding to $1.33 \cdot 10^{-5}/\sqrt{4} = 6.7 \cdot 10^{-6} \text{Hz}^{-1/2}$ (NEA). After subtracting the LIA noise, the random noise from detectors is $(6.7^2 - 4.46^2)^{1/2} \cdot 10^{-6} = 5 \cdot 10^{-6} \text{Hz}^{-1/2}$ (NEA). Therefore, each detector-preamplifier combination contributes a noise of $5 \cdot 10^{-6}/\sqrt{2} = 3.54 \cdot 10^{-6} \text{Hz}^{-1/2}$ (NEA). In addition, by removing a LIA board from Fig. 3 (a), the total noise in a single pass system of $2.52 \cdot 10^{-5} \text{Hz}^{-1/2}$ (NEA) is recorded. Hence, by subtracting the detector and LIA noises, we demonstrate the DFB laser noise of $(25.2^2 - 4.46^2 - 3.54^2)^{1/2} \cdot 10^{-6} = 2.45 \cdot 10^{-5} \text{Hz}^{-1/2}$ (NEA). The data shows the dominance of laser noise in a single pass WMS system. It means that the diode laser noise should be eliminated prior to the others.

In all random noises discussed above, the effect of the multi-pass cell has not been mentioned. Due to its large number of reflections and probable blemishes in the mirrors, there are numerous noises generating mechanisms, such
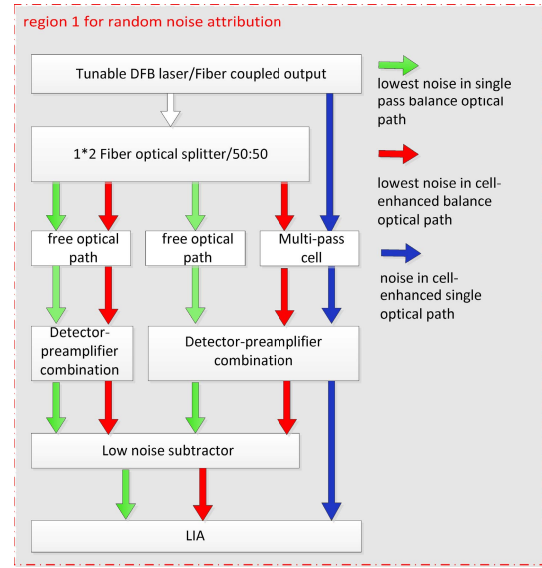

Fig. 5. The WMS arrangements with different noise properties.

TABLE I
RANDOM NOISE DISTRIBUTION OF THE SYSTEM

Noise distribution	NEA $(\text{Hz}^{-1/2})$	Corresponding concentration.length (CO, ppmv.m, 4 Hz bandwidth)
Noise in cell-enhanced single optical path (see the detail in Fig. 5)	$3.23 \cdot 10^{-5}$	250
LIA noise	$4.46 \cdot 10^{-6}$	34
Detector-amplifier combination noise	$3.54 \cdot 10^{-6}$	27
DFB Laser noise (RIN)	$2.45 \cdot 10^{-5}$	189
Cell-induced noise	$2 \cdot 10^{-5}$	155
Lowest noise in single pass balance optical path (see the detail in Fig. 5)	$6.7 \cdot 10^{-6}$	52
Lowest noise in cell-enhanced balance optical path (see the detail in Fig. 5)	$2.1 \cdot 10^{-5}$	162

as random laser speckle and etalon fringe which vary in response to changing ambient temperature and mechanical stress [12], [13]. Actually, the WMS detection limit depends on these interferences beside of laser noises, especially for the systems working in the field condition. Several methods such as purposed mechanical vibration [14], the double-modulation methods [15], [16] and data processing [11], [17]–[21] are reported to reduce the cell-induced interferences. In our system, the cell-induced noise is measured by using a 17.5 m White cell in Fig. 1. The recorded random noise is $6.46 \cdot 10^{-5}$ with bandwidth of 4 Hz, which indicates a cell-induced noise of $((6.46/\sqrt{4})^2 - 2.52^2)^{1/2} \cdot 10^{-5} = 2 \cdot 10^{-5} \text{Hz}^{-1/2}$ (NEA).

As a summary, the noise distribution of our WMS system is shown in Fig. 5 and Table 1.

According to the random noises in different arrangements, one can optimize the setup for specific applications. For instance, the balance detection is preferable in a single pass scheme due to the strong excess noise from the DFB laser. Besides, by comparing the lowest noises in balance path schemes with and without multi-pass cell, the single pass scheme with a path length of $17.5/(2.1/0.67) = 5.6$ *m* is equivalent to the cell-enhanced system. It means that comparing to our 17.5 m White type cell, one should use the

single pass scheme to achieve better SNR when the single pass optical length longer than 5.6 m is acceptable. It is noted that this result depends on the instruments in the system. New measurements are needed for different cell or diode laser, since the reference path may be unnecessary if the laser noise is relatively small.

IV. SIGNAL DRIFT ANALYSIS

In addition to the random noise which affects the SNR, slow signal drift is the major limit of long term precision due to its large amplitude. Many factors including the wavelength drift, the etalon fringe drift, and the change of self-mixing interference in the laser [22] can produce signal drift.

Firstly, the etalon fringe caused by the multi-pass cell is considered. Whilst vibration and double-modulation will result in rapid fringe change, it can be reduced by using longer integration time. In contrast, temperature fluctuation results in slow fringe change, especially when the fringe has large free spectral range (FSR). A number of technologies are reported to minimize these drift effects, such as rapid background subtraction or data processing [23], [24]. However, it is too expensive to implement the rapid background subtraction in field condition. In addition, it is difficult to deliver a stability improvement in the data processing when the signal drift has spectral range similar to the absorption linewidth. Furthermore, nonlinear tuning curves of the diode laser and several fringes with different FSRs also make the digital filters inefficient [24].

In [22], D. Masiyano et al. introduced self-mixing induced signal drift. For different types of lasers such as the Fabry-Perot laser, the DFB laser and vertical-cavity surface emitting laser (VCSEL), self-mixing interference can be caused by returned light from a flat mirror or a rough surface. In a WMS system, the self-mixing interference is different with the etalon fringe. Firstly, specular and diffuse reflections can result to self-mixing interference for the same levels. Secondly, for a DFB laser with package monitor detector, the self-mixing caused by the laser diode and the monitor detector will affects the absorption signal, whereas the etalon effect between them is absent. These properties make the self-mixing interference very difficult to eliminate.

For the long term stability analysis, a WMS model is established based on some reported literatures [25]–[29]. In WMS, the light intensity and wavelength are both modulated and there is a phase difference between them (WM/IM). In addition, the nonlinear modulation of the light intensity introduces higher harmonics, which the second is especially relevant. Therefore, the incident light intensity and frequency can be expressed as:

$$I(t) = I_0[1 + i_1 \cos(\omega t + \psi_1) + i_2 \cos(2\omega t + \psi_2)] \quad (1)$$
$$v(t) = v_0 + a \cos \omega t \quad (2)$$

where I_0, v_0 represent the mean light intensity and frequency driven by DC and saw-tooth currents, i_1 and i_2 are the amplitudes (normalized by I_0) of the linear and the first term of nonlinear intensity modulation, a is the frequency modulation depth, ω represents the regular frequency of modulation current, and ψ_1 and ψ_2 are the phase shifts between the wavelength modulation and the intensity modulation at two harmonic frequencies, respectively.

In WMS, the optical transmission coefficient can be viewed as a small variation in a constant value due to the weak absorption:

$$T(v) \approx 1 - \alpha(v) \quad (3)$$

In (3), the spectral absorbance $\alpha(v)$ can be expanded as:

$$-\alpha(v_0 + a \cos \omega t) = \sum_{k=0}^{\infty} H_k(v_0, a) \cos(k\omega t) \quad (4)$$

where functions H_k are the coefficients of harmonic frequencies (see the detail in [28]) which are proportional to $\alpha(v)$.

According to (1), (3) and (4), with the help of the background knowledge:

a. only DC terms in the multiplication output can survive from the RC filter in the LIA
b. the absorption is very small (generally smaller than 10^{-3}), thus $H_0 \ll 1$
c. for the modulation index of around 2.2, high order (>3) H_k terms can be ignored

the 2f spectral signal can be represented as:

$$S_{2f} = \frac{GI_0}{2}[H_2 + \frac{i_1}{2}(H_1 + H_3)\cos \psi_1 + i_2 \cos \psi_2] \quad (5)$$

where G is optical-electrical gain. The absorption is revealed by H_k functions. The last term is referred to the residual amplitude modulation (RAM). According to (5), the 2f background is decided by i_1, i_2, ψ_1, ψ_2 and H_k. Besides, the experiment demonstrates the background shift in response to changing laser temperature, which indicates the H_k domination of the background.

The drift analysis experiment is setup as shown in Fig. 6 (a). Figure (b) shows the slow changes of 2f spectral signals for high concentration CO (70000 ppmv.m, red) and free optical path (black) in 2 hours. The important observation is that, though the original signals in two optical paths are greatly different, their drifts are very similar. It means that the long term drift is mainly the background drift. According to the discussion in the last section, it should be attributed to the change of H_k, which can be caused by the diode laser or the optical path. In addition, since an optical path is free air which has flat spectral feature, the change of H_k mainly result from the diode laser.

The top figure of Fig. 6 (b) shows the fringe width of about 6 GHz, which corresponds to a cavity spacing of around 25 mm. According to the laser package length of about 20 mm, the long term distortion probably result from the change of the etalon fringes or the self-mixing interferences between the diode laser and the monitor diode or other points in the pigtail fiber. Therefore, it can be reduced in balance signal since the common spectral features in two optical paths are eliminated.

The signal in balance optical path (Fig. 6 (a) without the CO cell) is recorded in 8 hours, shown in Fig. 7. Assume that S_{a1}, S_{b1} are original signals from two optical paths respectively, S_{a2} and S_{b2} represent the signals 8 hours later. Then the
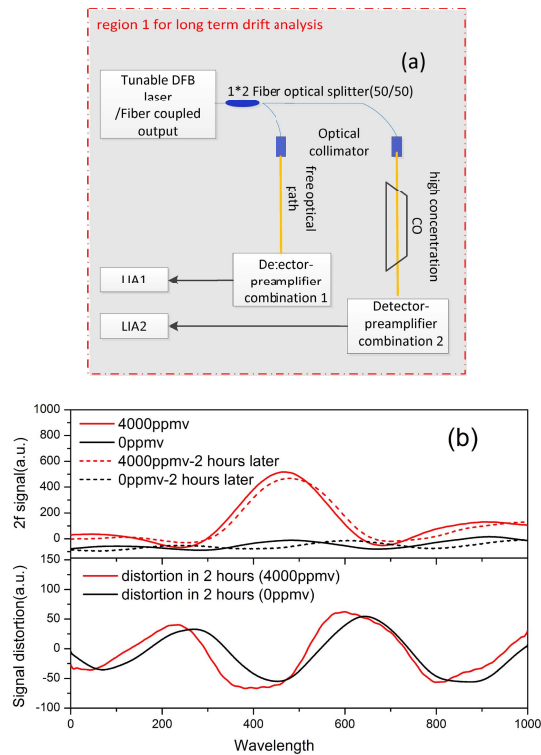
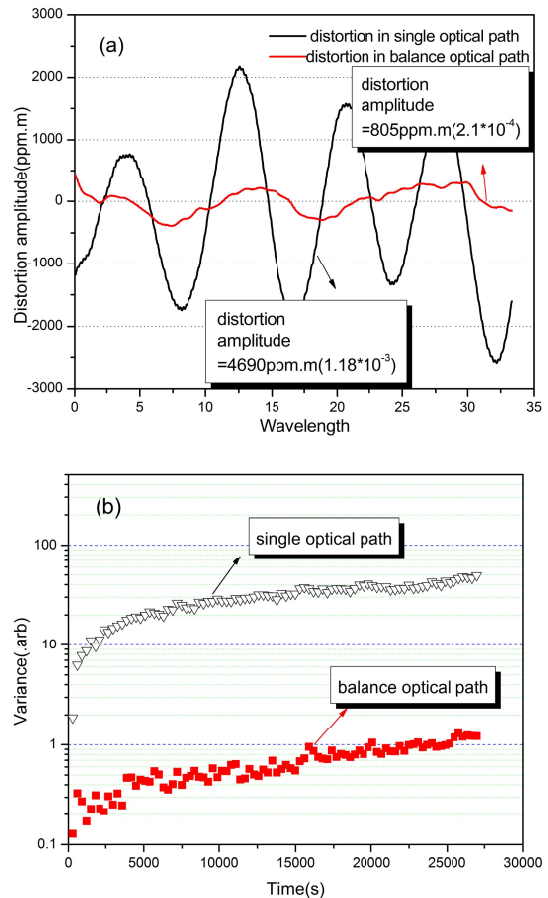Fig. 6. Long term drifts of different concentration CO in 2 hours.

Fig. 7.   Long term drift measurement of the balance optical path for 8 hours. (a) Shows signal drift in balance optical path and single optical path, respectively. (b) Shows corresponding variance.

drift in each optical path is $S_{a2} - S_{a1}$ or $S_{b2} - S_{b1}$ and the drift in balance optical path is $(S_{b2} - S_{b1}) - (S_{a2} - S_{a1})$. The data shows signal drift equivalent absorbance of $1.18 \cdot 10^{-3}$ in the single optical path whereas $2.1 \cdot 10^{-4}$ in the balance optical path, which indicates 6 times long term drift suppression by using reference path. Fig. 7 (b) shows the variances of signal drifts in two schemes, which indicates 34 times variance suppression in the balance optical path (solid square points).

V. THE CO MEASUREMENT EXPERIMENT

Considering the noise reduction and long term stability improvement, a new CO detection experiment is set up as shown in Fig. 8. The laser with incident power of 11mW passes through an optical isolator to eliminate the light reflection. A fiber optical splitter is used to divide it into three parts. It passes ∼80% through a 17.5 m White cell to a PIN detector (Detector3), ∼10% onto Detector2 after making a single pass across the free air as reference optical path. The 2f spectral signals in path 2 and path 3 are normalized by their light intensities and form the balance signal, which is used to obtain the CO concentration. The third part of the output is sent to Detector1 after passing through a 10 cm pure CO cell for line-locking, which is done by monitoring the absorption line and adjusting the laser temperature. In the experiment, the pure nitrogen (N_2) is initially pumped into the cell to get the background. In addition, the 2f spectral signal of 500 ppmv CO is recorded as calibration after subtracting the background. Finally, 40 ppmv CO is measured over 8 hours. By subtracting the background and applying a least-squares fitting (LSF) of calibration line shape, the CO concentration is extracted, shown in Fig. 9.
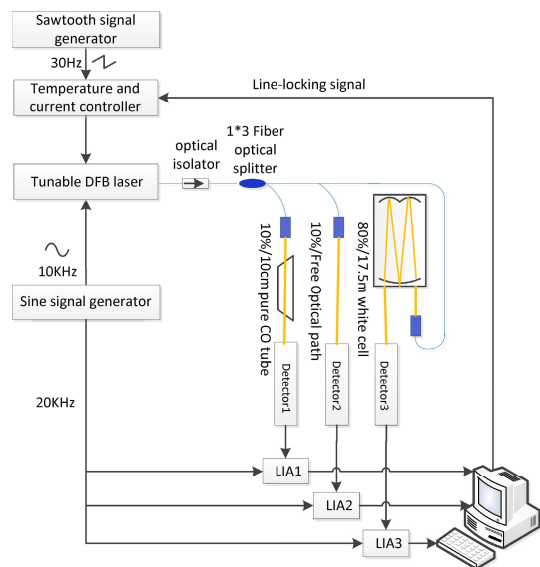

Fig. 8.   Experimental setup for CO measurement with line-locking loop and balance optical path.

Fig. 9 (a) shows similar detection sensitivity but significant drift reduction in the balance optical path. There is 20 ppmv long term drift in the balance optical path whereas 120 ppmv in the single optical path. All these data are in reasonably
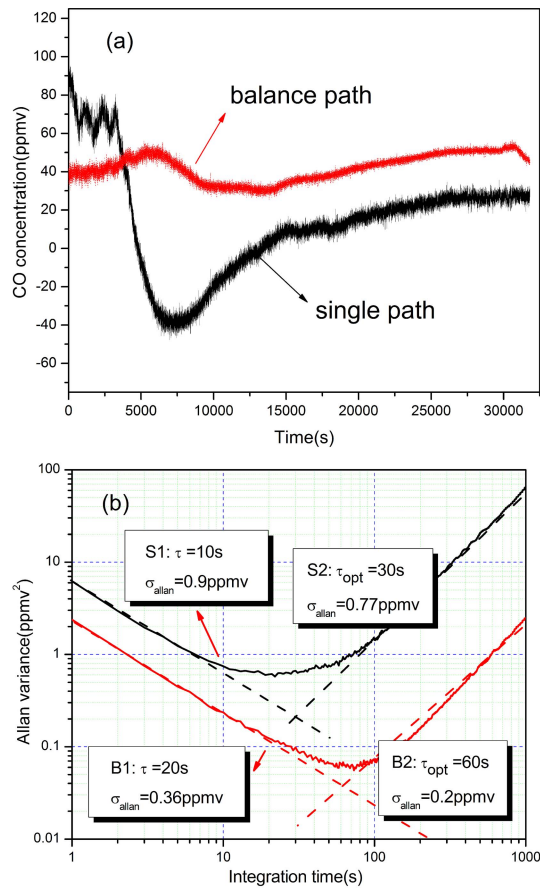
Fig. 9. Long term CO measurement in the balance optical path and single optical path: (a) is the concentration drift and (b) shows the Allan variance. It indicates twice the stability time in the balance optical path, which is 60 s contrasts to 30 s in the single optical path.

good agreement with the drift analysis in above sections. Fig. 9 (b) is the Allan variance [12], [13], [23], [24] which also indicates better stability performance in the balance optical path. The detection limits with 1 second integration time in the single optical path and balance path are 2.5 ppmv and 1.5 ppmv respectively, according to the first points in Allan curves. In addition, S1 and B1 show the detection limit of 0.36 ppmv with 20 seconds integration time in the balance path and 0.9 ppmv with 10 seconds integration time in the single path. Lower variance means lower noise in balance path, as the result of laser noise reduction. S2 and B2 indicate the longest useful integration time in two arrangements, which are 30 seconds in single path and 60 seconds in the balance path. This indicates twice the stability time in the balance optical path. However, for longer working time, the cell-induced drift should not be ignored since it increases with the time, and becomes the dominant source in the signal drift. Hence, the improvement of the cell robustness is currently under investigation.

VI. CONCLUSION

Possible reasons for random noise and long term signal drift in a typical 2f-detection TDLAS system are described in theory and measured in experiments. The noise distribution

in the system is obtained. The long term drift is proved to be mainly produced by slow changes in the spectral features of the diode laser. This also demonstrates significant stability improvement in the balance optical path system. However, the stability over the very long term is still limited by the multipass cell, and our subsequent works will focus on it. Finally, even though the detailed results depend on our experimental apparatus, a reliable insight into system optimization in specific applications is still provided by using the characterization process described in this paper.

REFERENCES

[1] P. Werle, "Spectroscopic trace gas analysis using semiconductor diode lasers," *Spectrochim. Acta A, Molecular Biomolecular Spectrosc.*, vol. 52, no. 8, pp. 805–822, 1996.

[2] W. A. Von Drasek, O. Charona, K. Mulderinka, D. M. Sonnenfroh, and M. G. Allen, "Multifunctional industrial combustion process monitoring with tunable diode lasers," *Proc. SPIE*, vol. 4201, p. 133, Feb. 2001.

[3] M. W. Sigrist, R. Bartlome, D. Marinov, J. M. Rey, D. E. Vogler, and H. Wächter, "Trace gas monitoring with infrared laser-based detection schemes," *Appl. Phys. B*, vol. 90, no. 2, pp. 289–300, 2008.

[4] P. A. Martin, "Near-infrared diode laser spectroscopy in chemical process and environmental air monitoring," *Chem. Soc. Rev.*, vol. 31, no. 4, pp. 201–210, 2002.

[5] H. Teichert, T. Fernholz, and V. Ebert, "Simultaneous *in situ* measurement of CO, H$_2$O, and gas temperatures in a full-sized coal-fired power plant by near-infrared diode lasers," *Appl. Opt.*, vol. 42, no. 12, pp. 2043–2051, 2003.

[6] K. Kunze, A. Zybin J. Koch, J. Franzke, M. Miclea, and K. Niemax, "Element selective detection of molecular species applying chromatographic techniques and diode laser atomic absorption spectrometry," *Spectrochim. Acta A, Molecular Biomolecular Spectrosc.*, vol. 60, no. 14, pp. 3393–3401, 2004.

[7] Z. Zhang *et al.*, "Simultaneous detection of multiple gas concentrations with multi-frequency wavelength modulation spectroscopy," *Europhys. Lett.*, vol. 104, no. 4, p. 44002, 2013.

[8] L. S. Rothman *et al.*, "The HITRAN 2012 molecular spectroscopic database," *J. Quant. Spectrosc. Radiat. Transf.*, vol. 130, pp. 1–400, Nov. 2013. [Online]. Available: http://www.cfa.harvard.edu/hitran/

[9] B. Lins, P. Zinn, R. Engelbrecht, and B. Schmauss, "Simulation-based comparison of noise effects in wavelength modulation spectroscopy and direct absorption TDLAS," *Appl. Phys. B*, vol. 100, no. 2, pp. 367–376, 2010.

[10] G. Tu *et al.*, "Novel method for correcting light intensity fluctuation in the TDLAS system," *Chin. Opt. Lett.*, vol. 10, no. 4, p. 042801, 2012.

[11] L. Persson, F. Andersson, M. Andersson, and S. Svanberg, "Approach to optical interference fringes reduction in diode laser absorption spectroscopy," *Appl. Phys. B*, vol. 87, no. 3, pp. 523–530, 2007.

[12] M. B. Frish, R. T. Wainner, M. C. Laderer, K. R. Parameswaran, D. M. Sonnenfroh, and M. A. Druy, "Precision and accuracy of miniature tunable diode laser absorption spectrometers," *Proc. SPIE*, vol. 8032, p. 803209, May 2011.

[13] J. Hodgkinson, D. Masiyano, and R. P. Tatam, "Gas cells for tunable diode laser absorption spectroscopy employing optical diffusers. Part 1: Single and dual pass cells," *Appl. Phys. B*, vol. 100, no. 2, pp. 291–302, 2010.

[14] V. V. Liger, "Optical fringes reduction in ultrasensitive diode laser absorption spectroscopy," *Spectrochim. Acta A, Molecular Biomolecular Spectrosc.*, vol. 55, no. 10, pp. 2021–2026, 1999.

[15] A. Zybin, C. Schnürer-Patschan, and K. Niemax, "Wavelength modulation diode laser atomic absorption spectrometry in modulated low-pressure helium plasmas for element-selective detection in gas chromatography. Plenary lecture," *J. Anal. Atomic Spectrometry*, vol. 10, no. 9, pp. 563–567, 1995.

[16] C. Dyroff *et al.*, "Stark-enhanced diode-laser spectroscopy of formaldehyde using a modified Herriott-type multipass cell," *Appl. Phys. B, Lasers Opt.*, vol. 88, no. 1, pp. 117–123, 2007.

[17] H. Xia, G. Tu, T. Pang, Z. Zhang, B. Wu, and F. Dong, "Improvement of tunable diode laser absorption system with a novel multipass cell and wavelet transform," *J. Meas. Sci. Instrum.*, vol. 2, no. 4, pp. 402–405, 2011.

[18] J. Li, U. Parchatka, and H. Fischer, "Applications of wavelet transform to quantum cascade laser spectrometer for atmospheric trace gas measurements," *Appl. Phys. B*, vol. 108, no. 4, pp. 951–963, 2012.

[19] J. Li, B. Yu, W. Zhao, and W. Chen, "A review of signal enhancement and noise reduction techniques for tunable diode laser absorption spectroscopy," *Appl. Spectrosc. Rev.*, vol. 49, no. 8, pp. 666–691, 2014.

[20] P. W. Werle, P. Mazzinghi, F. D'Amato, M. De Rosa, K. Maurer, and F. Slemr, "Signal processing and calibration procedures for *in situ* diode-laser absorption spectroscopy," *Spectrochim. Acta A, Molecular Biomolecular Spectrosc.*, vol. 60, nos. 8–9, pp. 1685–1705, 2004.

[21] D. S. Bomse and D. J. Kane, "An adaptive singular value decomposition (SVD) algorithm for analysis of wavelength modulation spectra," *Appl. Phys. B*, vol. 85, nos. 2–3, pp. 461–466, 2006.

[22] D. Masiyano, J. Hodgkinson, S. Schilt, and R. P. Tatam, "Self-mixing interference effects in tunable diode laser absorption spectroscopy," *Appl. Phys. B*, vol. 96, no. 4, pp. 863–874, 2009.

[23] A. Fried, B. Henry, B. Wert, S. Sewell, and J. R. Drummond, "Laboratory, ground-based, and airborne tunable diode laser systems: Performance characteristics and applications in atmospheric studies," *Appl. Phys. B*, vol. 67, no. 3, pp. 317–330, 1998.

[24] P. Werle, "Accuracy and precision of laser spectrometers for trace gas sensing in the presence of optical fringes and atmospheric turbulence," *Appl. Phys. B*, vol. 102, no. 2, pp. 313–329, 2011.

[25] P. Kluczynski and O. Axner, "Theoretical description based on Fourier analysis of wavelength-modulation spectrometry in terms of analytical and background signals," *Appl. Opt.*, vol. 38, no. 27, pp. 5803–5815, 1999.

[26] P. Kluczynski, A. M. Lindberg, and O. Axner, "Background signals in wavelength-modulation spectrometry with frequency-doubled diode-laser light. I. Theory," *Appl. Opt.*, vol. 40, no. 6, pp. 783–793, 2001.

[27] P. Kluczynski, A. M. Lindberg, and O. Axner, "Background signals in wavelength-modulation spectrometry by use of frequency-doubled diode-laser light. II. Experiment," *Appl. Opt.*, vol. 40, no. 6, pp. 794–805, 2001.

[28] H. Li, G. B. Rieker, X. Liu, J. B. Jeffries, and R. K. Hanson, "Extension of wavelength-modulation spectroscopy to large modulation depth for diode laser absorption measurements in high-pressure gases," *Appl. Opt.*, vol. 45, no. 5, pp. 1052–1061, 2006.

[29] M. Gharavi and S. G. Buckley, "A multiplexed diode laser sensor based on wavelength modulation spectroscopy for simultaneous measurement of temperature and concentration of H_2O and CH_4," in *Proc. 4th Joint Meeting U.S. Sec. Combustion Inst.*, Philadelphia, PA, USA, Mar. 2005, p. 17.

Guojie Tu received the B.Sc. degree in applied physics from Anhui University, Hefei, China, in 2007, and the Ph.D. degree in optics from the Anhui Institute of Optics and Fine Mechanics, Chinese Academy of Sciences, Hefei, in 2012. His research has been focusing on atmospheric trace gases detection using tunable diode laser absorption spectroscopy technique and optic fiber sensing.

Fengzhong Dong received the Degree from Nankai University, Tianjin, China, in 1986, and the M.Sc. and Ph.D. degrees from the Anhui Institute of Optics and Fine Mechanics (AIOFM), Chinese Academy of Sciences (CAS), Hefei, China, in 1989 and 1992, respectively. After working with the Institute of Physics, CAS, for a short period, he joined the Foundation for Research and Technology of Hellas, Crete, Greece, as a Visiting Scientist. Since 1996, he has been with the Centre for Microsystems and Photonics, University of Strathclyde, Glasgow, U.K., as a Senior Research Fellow. He is currently a Professor with AIOFM, CAS. His major interests have been focusing on environmental pollution monitoring, industrial process control, and fiber sensing.

Yu Wang received the B.Sc. degree in remote sensing from the Harbin Institute of Technology, Harbin, China, in 1993, and the Ph.D. degree in electronics engineering from the University of Strathclyde, Glasgow, U.K., in 2005. He was with the China Aerospace Science and Industry Corporation, Beijing, China, as an Engineer, from 1993 to 1999. He is currently a Professor with the Key Laboratory of Environment Optics and Technology, Chinese Academy of Sciences, Hefei, China. His major research interest focuses on photoelectric detection.

Brian Culshaw received the Ph.D. degree in electronic and electrical engineering with specialization in microwave semiconductors, in 1969. He held appointments at Cornell University, Ithaca, NY, USA, in 1970, Bell Northern Research, Ottawa, ON, Canada, from 1971 to 1973, University College London, from 1974 to 1983, and Stanford University, in 1982, and has been a Professor of Electronics at the University of Strathclyde, Glasgow, U.K., since 1983. His personal research activities have centered upon optical fiber sensor system and network studies and novel technologies for optical fiber instrumentation, including pressure measurement systems, strain and temperature measuring systems, gyroscopes, and structural assessment techniques.

Zhirong Zhang was born in 1981. He received the Ph.D. degree, and was a Research Associate. He is currently with the Anhui Provincial Key Laboratory of Photonic Devices and Materials, Anhui Institute of Optics and Fine Mechanics, Chinese Academy of Sciences, Hefei, China. His major research interest is focusing on the development of novel spectroscopic detection technologies for applications in environmental monitoring and industrial process control.

Tao Pang received the B.Sc. and M.Sc. degrees from Northwest Polytechnical University, Fremont, CA, USA, in 2006 and 2009, respectively. He joined Anhui Institute of Optics and Fine Mechanics, Chinese Academy of Sciences, Hefei, China, as a Research Assistant.

Hua Xia received the B.Sc. degree in physics from Henan University, Kaifeng, China, in 2007, and the Ph.D. degree from the Anhui Institute of Optics and Fine Mechanics, Chinese Academy of Sciences, Hefei, China, in 2012. Her research has been focusing on trace gas detection using TDLAS technique.

Bian Wu was born in 1972. He received the Ph.D. degree and was an Associate Professor. He is currently with the Anhui Institute of Optics and Fine Mechanics, Chinese Academy of Sciences, Hefei, China. His main research directions are in laser technique and the optics mechanical design.